# Methylomes reveal recent evolutionary changes in populations of two plant species

Kevin Korfmann[ab1], Andreas Zauchner[a1], Bing Huo[a], Corinna Grünke[a], Yitong Wang[a], Aurélien Tellier[a†2], Ramesh Arunkumar [a†2]

[a]Section of Population Genetics, School of Life Sciences, Technical University of Munich, Liesel-Beckmann Strasse 2, 85354 Freising, Germany

[b]Present address: Department of Biology 77 Klamath Hall 1210 University of Oregon Eugene, OR 97403

[1] These authors contributed equally

[2] These authors contributed equally

[†] Authors for correspondence (Aurélien Tellier - aurelien.tellier@tum.de, Ramesh Arunkumar – arunkumar.ramesh@tum.de)

**Abstract**

Plant DNA methylation changes occur hundreds to thousands of times faster than DNA mutations and can be transmitted transgenerationally, making them useful for studying population-scale patterns in clonal or selfing species. However, a state-of-the-art approach to use them for inferring population genetic processes and demographic histories is lacking. To address this, we compare evolutionary signatures extracted from CG methylomes and genomes in *Arabidopsis thaliana* and *Brachypodium distachyon*. While methylation variants (SMPs) are less effective than genetic variants (SNPs) for identifying population differentiation in *A. thaliana*, they can classify phenotypically divergent *B. distachyon* subgroups that are otherwise genetically indistinguishable. The site frequency spectra generated using methylation sites from varied genomic locations and evolutionary conservation exhibit similar shapes, indicating minimal noise when all CG sites are analyzed jointly. Nucleotide diversity is three orders of magnitude higher for methylation variants than for genetic variants in both species, driven by the higher epimutation rate. Correlations between SNPs and SMPs in nucleotide diversity and allele frequencies at gene exons are weak or absent in *A. thaliana*, possibly because the two sources of variation reflect evolutionary forces acting at different timescales. Linkage disequilibrium quickly decays within 250 bp for methylation variants in both plant species. Finally, we developed a deep learning-based demographic inference approach. We identified recent population expansions in *A. thaliana* and *B. distachyon* using methylation variants that were not identified when using genetic variants. Our study demonstrates the unique evolutionary insights methylomes provide that genetic variation alone cannot reveal.

**Keywords:** Methylation site frequency spectra, demographic inference, deep learning, Tajima's *D*, linkage disequilibrium, nucleotide diversity, clocklike regions, gene body methylation, *Arabidopsis thaliana*, *Brachypodium distachyon*

## Background

Understanding how variation is partitioned within and between populations is a central goal in evolutionary biology. Increasing evidence suggests that epigenetic modifications can vary within and between populations [1]. Nevertheless, our knowledge of how epigenomes evolve through neutral and selective forces and, consequently, their capacity to reveal population demographic histories is limited. DNA cytosine methylation, a conserved epigenetic modification in eukaryotes [2], occurs in plants within three sequence contexts: CG, CHG, and CHH (H represents A, T, or C) [3]. DNA methylation is known to be involved in regulating gene expression, suppressing transposable element activity, and stabilizing the genome [3]. Long-term changes in the methylome are mainly shaped by genomic alterations such as the proliferation of transposable elements and mutations affecting DNA methylation pathways, whereas heritable stochastic epimutations that occur independent of genomic background drive short-term changes [4].

The unique characteristics of epimutations make them appealing markers for evolutionary investigations. In plants, CG methylation is maintained during cell division by METHYLTRANSFERASE 1 (MET1) [3]. Spontaneous stochastic loss or gain of methylation at CG sites can be transmitted stably across multiple generations [5]. Van der Graaf *et al*. have estimated the forward (gain of DNA methylation) and backward (loss of methylation) epimutation rates per CG site in the model plant *Arabidopsis thaliana* to be approximately $2.56\times10^{-4}$ and $6.3\times10^{-4}$, respectively, per generation per haploid methylome [6]. These rates are several orders of magnitude higher than the mutation rate of $7\times10^{-9}$ base substitutions per site per generation in the same population [7]. The increased rates of change at the epigenetic level may facilitate evolutionary inference over recent timescales, where the utility of slower-evolving genetic markers is limited [8, 9].

As transiently induced epimutations can be mistaken for stably inherited markers, a recent study exposed genetically identical *A. thaliana* to various environmental conditions to identify

genomic regions—termed clocklike regions—where CG divergence rates are independent of environmental stimuli [10]. While these regions are valuable for evolutionary studies, they are challenging to identify in most species. Therefore, the same study observed that gene body methylated regions (gbM) exhibit a pattern similar to that of CG divergence in clocklike regions [10]. gbM refers to a subclass of genes that display elevated CG methylation. They are mostly found in moderately and constitutively expressed housekeeping genes [11]. As they can be identified based on the distribution of methylation in the gene bodies, their use may facilitate the investigation of evolutionary processes in nonmodel plant species.

Previous attempts to explore how methylation variants evolve have either neglected demographic (neutral) models, mixed environmentally sensitive and insensitive methylation sites, or did not adequately assess the interdependence of genetic and methylation variants. Charlesworth and Jain's analytic framework for hypermutable sites [12] has been applied to create a methylation site frequency spectrum (mSFS) [4]. Previous studies generated mSFS for genic CG sites and the methylation states of gbM genes, finding either no selection or only weak selection acting on the methylome in *A. thaliana* [4, 13] and maize [14]. However, these studies do not incorporate an explicit demographic model while assessing selection. Another study found that positive selection acted on methylation variants linked to metabolite regulation in *A. thaliana*, even after accounting for demographic histories [15]. Other studies in *Brachypodium distachyon* [16], *Fragaria vesca* [17, 18], lettuce [19], and grapevines [20] have compared evolutionary inferences using genetic and methylation variants by analyzing all CG sites as the environmental sensitivity of individual sites is unknown in most plant species. Recently, Sellinger *et al*. utilized methylation as a secondary marker alongside genetic variants to enhance demographic inference over short and long timescales [8]. The conceptual novelty was to consider that the underlying genealogy at a locus (*i.e.* the coalescent tree tracing back the ancestry of the sample back in time) is common for SNPs and SMPs (under a neutral model of evolution). This represents the first population genomics inference model combining DNA mutations, epimutations, and recombination along the genome, and the basis for

developing a Sequential Markovian Coalescent method (SMCm). However, that study exhibits a fair amount of noise in the inference of past evolutionary history when it was applied to methylome data from *A. thaliana* [8]. These inaccuracies are due to a lack of knowledge about the optimal SMP markers to use, the relevant genomic context, the relationship between SNPs and SMPs, and the SMCm method being very sensitive and not accounting well for methylated region effects (so-called differentially methylated regions or DMRs). A related question is whether DMRs can be used for evolutionary inferences as well.

Given these limitations, our goal was to assess how well methylation variants reveal known evolutionary patterns inferred using genetic variants. We chose *A. thaliana* and *B. distachyon* for our analyses because their evolutionary histories are well-described [16, 21]. We found that the capacity of methylation variants to differentiate populations is contingent on when populations diverge. We also show that CG sites across the methylome capture within- and between-population patterns comparable to environmentally insensitive sites (clocklike regions and gbM) [10] in samples grown in a common garden. We found weak or no local correlations between genetic and methylation variants, indicating they reflect different aspects of population evolutionary histories. Additionally, the linkage between neighboring methylation variants was minimal. Conventional genome-based demographic inference methods, such as the Sequential Markovian Coalescent [22], show limitations in using methylation variants due to high sensitivity to violations of the Markovian properties of the underlying coalescent model along the genome [8]. Moreover, since such methods require knowing the variant accumulation rates and distributions—often unknown for methylation in many species—we developed a deep learning method that uses methylation as a neutral marker to estimate past demography. Unlike conventional convolutional networks, we use (to our knowledge) the first Encoder-Only Transformer architecture [23-25] method, focusing on the placement of mutations on a hidden ancestral recombination graph. We track estimates of coalescent events in a time-discretized transition matrix by using heterogeneous sites per genomic window as input, thereby applying a coarse-grained approach, similar to tsABC [22]. By

aligning training and real data distributions, we show that rapidly changing methylation variants can reveal recent demographic shifts in selfing and clonal species.

## Results

### CG methylation variants have variable performance in identifying population structure

We analyzed genetic and methylation diversity using 63 samples each from the Central European (CEU) and the Iberian non-relicts (IBnr) *A. thaliana* populations (Table S1). These populations were used by Strütt *et al*. [22]. Across the two populations, 31-33% of CG methylation sites in clocklike regions were polymorphic (Figure S1A), which is similar to a previous estimate for CG sites in *A. thaliana* mutation accumulation lines [26]. In contrast, 1.6-1.7% of coding sites and 2.7-2.8% of non-coding sites were polymorphic (Figure S1A). We compared our results from *A. thaliana* with those from 29 samples from the clonally propagating grass *B. distachyon*. Wilson *et al*. used SNPs to identify clonal groups among Turkish *B. distachyon*, with samples within each group showing high levels of genetic similarity [27]. Eichten *et al*. identified high levels of consistency between the known genetic relationships for the clonal groups and the extent of CG divergence [16]. Here, we restrict our focus to SMPs and DMRs occurring within gbM regions and two clonal groups of *B. distachyon* with average bisulfite sequencing depths greater than 10 [16] (Group 1: 22 samples, Group 6: 7 samples) (Table S1). Between 4-7% of CG methylation sites within gbM regions were polymorphic in *B. distachyon* (Figure S1B). The median length of DMRs in *B. distachyon* was 107 bp ($1^{st}$ percentile: 44 bp, 99% percentile: 717 bp) which is smaller than the median length in *A. thaliana* DMRs, which was 181 bp ($1^{st}$ percentile: 78 bp, 99% percentile: 1125 bp) (Figure S2).

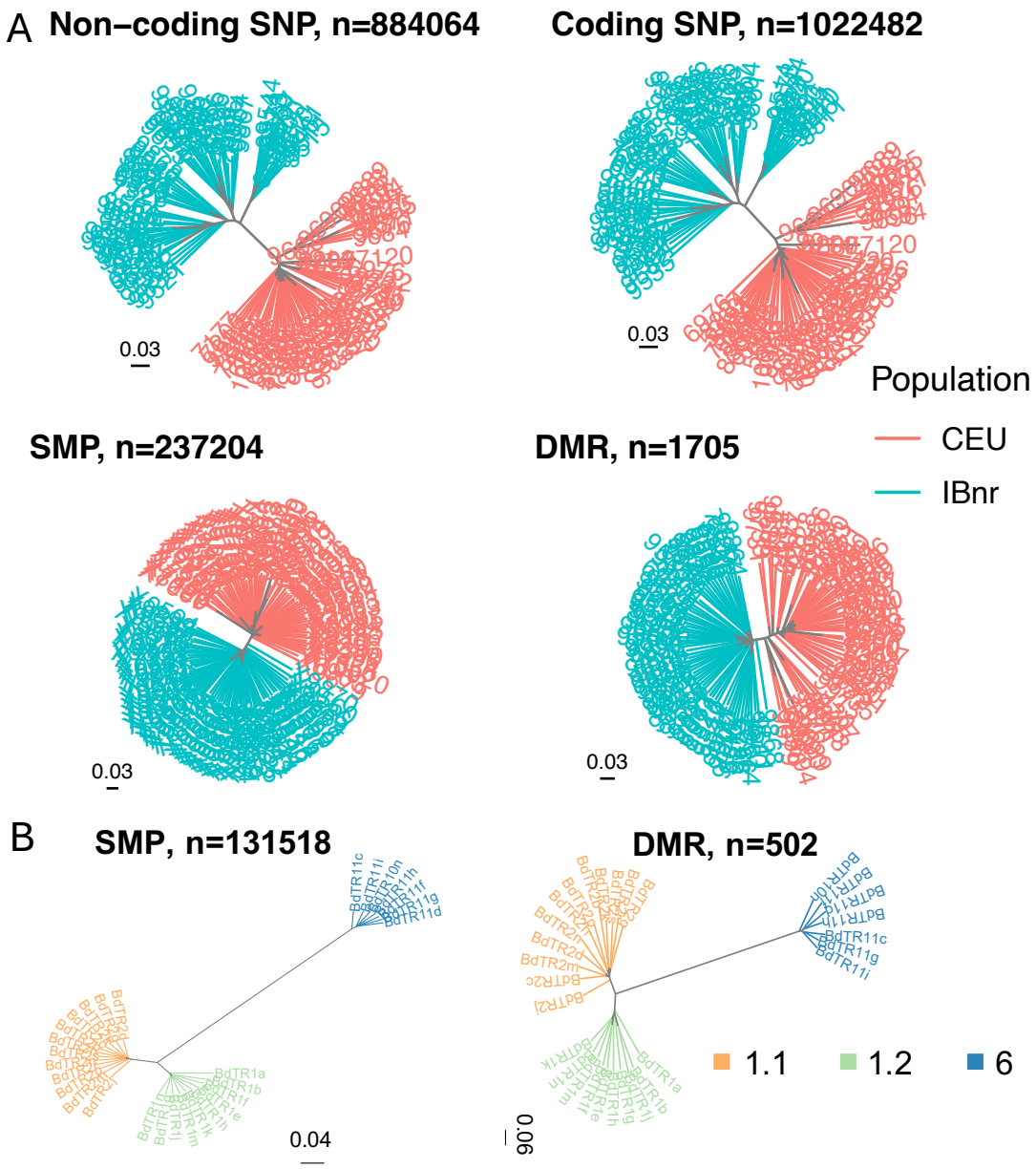


**Figure 1**. Methylomes outperform genetic variants in detecting population subdivision in *Brachypodium distachyon* but not *Arabidopsis thaliana*. (**A**) Neighbor-joining trees were generated using p-distance matrices for non-coding single nucleotide polymorphisms (SNP), coding SNPs, clocklike region single methylation polymorphisms (SMP), and clocklike region differentially methylated regions (DMR) for Central European (CEU) and the Iberian non-relicts (IBnr) *A. thaliana*. (**B**) Neighbor-joining trees generated using p-distance matrices estimated for SMP and DMR in gbM regions of Turkish *Brachypodium distachyon* clonal groups.

178 We estimated the proportion of sites at which two samples were different (p-distance) and
179 clustering to uncover how the net total of genetic and methylation variation differed between
180 samples from the CEU and IBnr populations. In this approach, a clear separation between the
181 CEU and IBnr populations was apparent with both coding and non-coding single nucleotide
182 polymorphisms (SNP) (Figure 1A). Although single methylation polymorphisms (SMP) and
183 differentially methylated regions (DMR) largely separated the two populations, some samples
184 were separated by only minimal distances (Figure 1A). Clustering indicated nine or more
185 groups within the SNP data (Figure S3A-B), whereas only two groups were apparent in the
186 SMP and DMR datasets (Figure S3C-D).
187
188 Furthermore, we performed discriminant analysis of principal components (DAPC) analyses
189 to identify how correlated changes in subsets of genetic and methylation variants can be used
190 to discriminate the two populations. DAPC indicated greater discriminatory power with coding
191 and non-coding SNPs compared to SMPs and DMRs (Figure S3E). Although p-distance
192 matrix-based comparisons could have been influenced by the greater number of SNPs (Figure
193 1A), marker numbers were comparable for the DAPC, and yet SMPs and DMRs showed poor
194 discriminatory capability (Figure S3E). SMPs and DMRs that occur within gbM genes have
195 comparable performance to those occurring within clocklike regions in discriminating the two
196 populations (Figure S4). High methylation rates in *A. thaliana* may have caused multiple
197 changes at the same site (so-called homoplasy accounted for as a finite site model [4, 12,
198 28]), resulting in the underestimation of the true levels of divergence. Indeed, the divergence
199 between IBnr and CEU populations is estimated to have occurred after the last glacial
200 maximum ca. 10,000-20,000 years ago [29-31].
201
202 We then performed a similar analysis using the *B. distachyon* accessions. In contrast to the
203 clonal grouping based on the genetic profiles [27], SMPs and DMRs were capable of
204 additionally distinguishing the two subgroups of Group 1 (Figures 1B, S5). The trees estimated
205 using the p-distance matrices were shorter for SMPs compared to DMRs (Figure 1B), possibly

206 due to increased error in this dataset because of the shallow bisulfite sequencing depths.
207 However, both trees were longer compared to those in *A. thaliana* (Figure S4A) indicating
208 greater methylome differentiation in *B. distachyon*. Both our results using gbM regions and the
209 results from Eichten *et al*. that use the entire collection of CG sites [16] reveal a difference in
210 methylation profiles between the two subgroups of Group 1. We obtained phenotype data for
211 the two subgroups [32] and found significant differences in the longitude (Figure S6), elevation
212 of collection site, seed lengths, widths, yield production, and germination percentages (Figure
213 S7). Our findings suggest that methylation variants can reveal subpopulation structure in
214 recent timescales, where there has been little time for genetic differences and multiple
215 methylation changes to accumulate.
216
217 **Genomic contexts have little influence on the shape of SMP distributions**

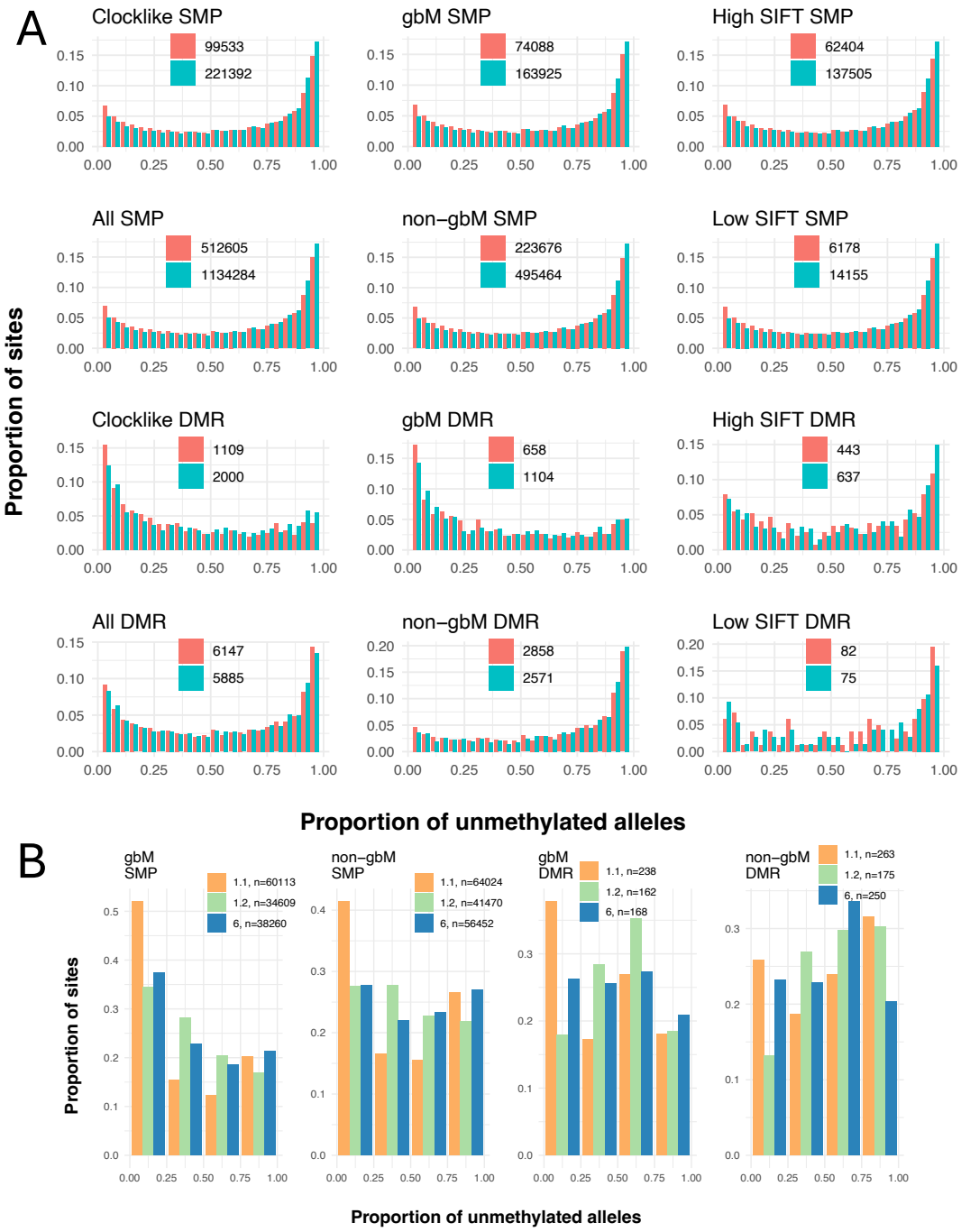


**Figure 2**. Methylation site frequency spectra generated using single methylation polymorphisms were similar regardless of genomic contexts. Methylation site frequency spectra (mSFS) generated using differentially methylated regions (DMR) exhibited greater variability. (**A**) mSFS for the Central European (CEU, Salmon) and the Iberian non-relicts (IBnr, Cyan) *Arabidopsis thaliana* populations using CG sites that occur in clocklike, gene body methylated (gbM), non-gbM, and low and high Sorting Intolerant from Tolerant (SIFT) score regions. Only sites with minor allele frequencies (MAF) >0.02 were used to generate the

226 mSFS. (**B**) mSFS for *Brachypodium distachyon* clonal groups 1.1, 1.2, and 6 for single
227 methylation polymorphisms (SMP) and DMRs occurring within gbM and non-gbM regions.
228 Only sites with minor allele frequencies (MAF) >0.04 were used to generate the mSFS. For
229 (A) and (B), the numbers in each panel indicate the number of sites used for the analyses.
230
231
232 We sought to understand how genomic contexts influenced the methylation site frequency
233 spectra (mSFS) in *A. thaliana*. The mSFS reveals how methylation rates, demographic
234 changes, and natural selection influence changes in the methylome over time [4, 12]. We
235 found a greater frequency of unmethylated alleles at most polymorphic methylation sites for
236 the CEU and IBnr populations, but CEU consistently had higher frequencies of unmethylated
237 alleles (Figure 2A). The shapes of the mSFS for SMPs are consistent with previous findings
238 that the backward methylation rate promoting the change from methylated to unmethylated is
239 higher than the forward rate [6] and are consistent with previous mSFS generated by
240 combining *A. thaliana* samples from extended geographic regions [4, 13]. The shape of the
241 mSFS for SMPs in clocklike and gbM regions were similar, supporting their interchangeability.
242 We also studied the mSFS for intervals containing genes with low and high Sorting Intolerant
243 From Tolerant (SIFT) scores, which are positively correlated with the level of evolutionary
244 constraint that genes are under [33]. Our results indicate that the level of gene constraint has
245 little impact on the mSFS shape (Figure 2A).
246
247 When compared to SMPs, the DMR mSFS for *A. thaliana* were more dependent on the
248 underlying set of intervals used to generate them. For DMRs that occur in intervals containing
249 non-gbM genes and high and low SIFT-score genes, more samples have the unmethylated
250 state reflecting the underlying SMP distributions (Figure 2A). This is also true when DMRs
251 across the entire genome are analyzed (Figure 2A). In contrast, for DMRs in clocklike regions
252 and gbM genes, more samples exhibit the methylated state (Figure 2A). The mSFS shapes

253 for DMRs show greater variability compared to those for SMPs, which may reflect underlying
254 differences in their molecular basis.
255
256 In contrast to the mSFS for SMPs in *A. thaliana* (Figure 2A), the mSFS for all three clonal
257 groups of *B. distachyon* indicated an excess of methylated alleles within gbM and non-gbM
258 SMPs, although it was less pronounced for the latter (Figure 2B). There was less consistency
259 in the shapes of the mSFS for DMRs in gbM and non-gbM regions (Figure 2B), similar to our
260 observation when *A. thaliana* DMRs were analyzed (Figure 2A).
261
262 **Methylation and genetic variants show unique evolutionary signatures in *A. thaliana***

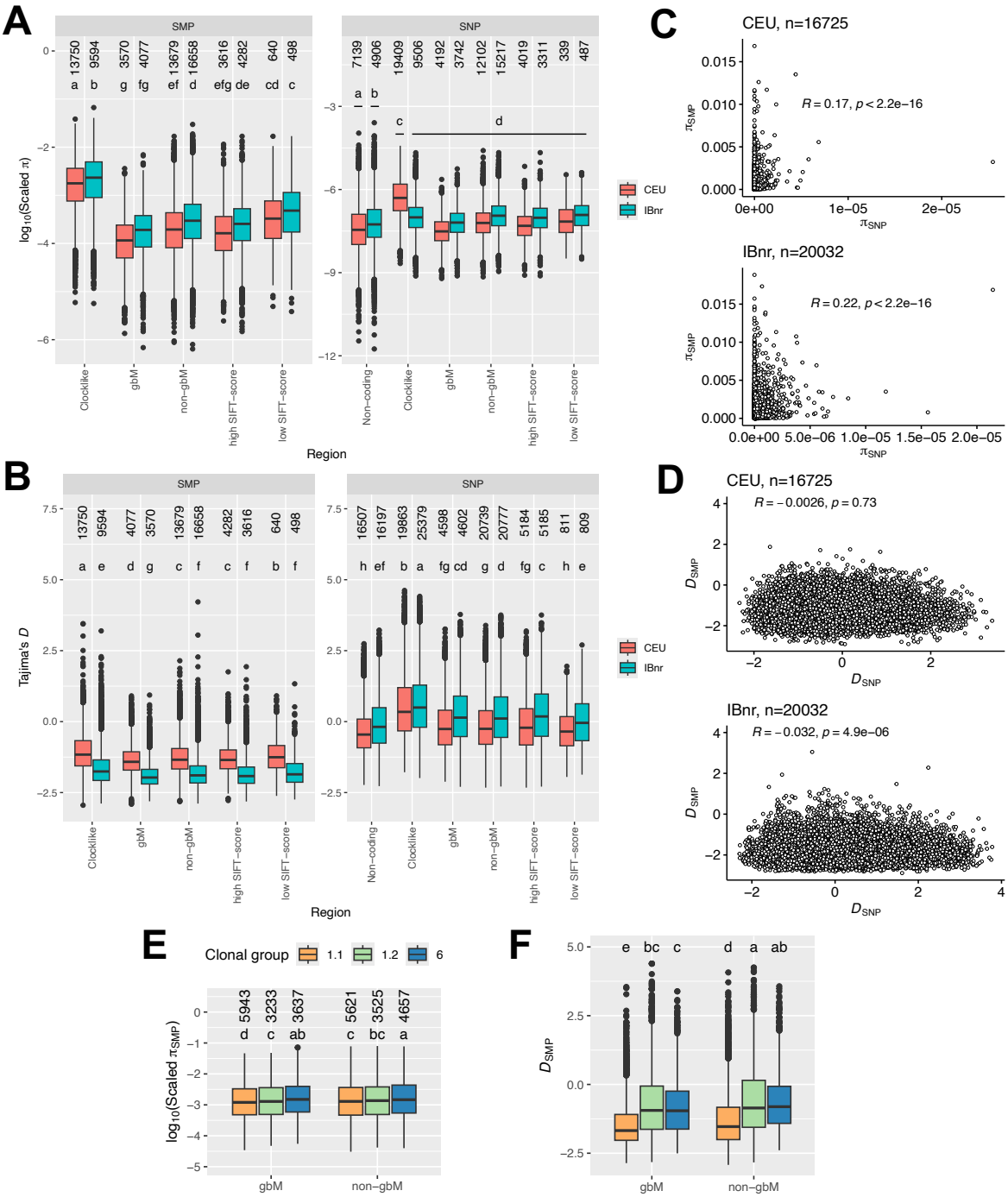


**Figure 3**. Unique evolutionary signatures in genomes and methylomes. (**A**) Estimates of pairwise nucleotide diversity (π) scaled by the number of cytosines per region for single methylation polymorphisms ($\pi_{SMP}$) and the number of bases for single nucleotide polymorphisms ($\pi_{SNP}$) for the Central European (CEU) and the Iberian non-relicts (IBnr) *Arabidopsis thaliana* populations. (**B**) Estimates of Tajima's *D* per region for CEU and IBnr. Comparisons of (**C**) $\pi_{SNP}$ versus $\pi_{SMP}$ and (**D**) Tajima's *D* for SNPs ($D_{SNP}$) and SMPs ($D_{SMP}$)

270 per gene for CEU and IBnr. The numbers in the titles of each panel indicate the number of
271 sites used for the analyses. Correlation tests were conducted to assess the associations
272 between π and Tajima's *D*. (**E**) $\pi_{SMP}$ scaled by the number of cytosines per region for
273 *Brachypodium distachyon* clonal groups 1.1, 1.2, and 6. (**F**) $D_{SMP}$ per region for *B. distachyon*.
274 For (A), (B), (E), and (F), the numbers above the boxplots indicate the number of intervals.
275 Letters indicate group-wise differences in means following Tukey's honest significant
276 difference tests. For (F), the color scheme and number of sites are the same as in (E).
277
278
279 We next sought to understand how genetic and methylation polymorphisms are distributed
280 within *A. thaliana* populations. We first calculated the pairwise nucleotide diversity (π) for
281 SMPs ($\pi_{SMP}$) and SNPs ($\pi_{SNP}$) from noncoding, clocklike, gbM, non-gbM, and high and low
282 SIFT genic regions. We scaled estimates by the total number of sites (polymorphic and
283 monomorphic) to ensure that the results were comparable (that is per-site estimates). $\pi_{SMP}$ is
284 three orders of magnitude higher than $\pi_{SNP}$ (Figure 3A), likely driven by the high rates of
285 change in methylomes [6]. $\pi_{SNP}$ in the CEU population and $\pi_{SMP}$ in CEU and IBnr populations
286 for clocklike regions were significantly higher than in other regions (Figure 3A), possibly
287 indicating better detection of environmental insensitivity with more polymorphic sites. $\pi_{SMP}$ was
288 higher for gbM and high-SIFT genes than at non-gbM and low-SIFT, respectively, but no such
289 difference was seen for $\pi_{SNP}$ (Figure 3A), indicating that constraint at the genic level has a
290 minor effect on the levels of local methylation diversity.
291
292 We then compared how selective and demographic processes influence genomes and
293 methylomes by estimating Tajima's *D* for CEU and IBnr. For methylomes, we used a modified
294 Tajima's *D* using the $D^m$ [28] that accounts for the hypermutability of the methylation sites.
295 $D_{SNP}$ was slightly negative for noncoding sites in the CEU and IBnr populations (Figure 3B),
296 reflecting the known history of population expansions [22]. The higher $D_{SNP}$ for IBnr (Figure
297 3B) is consistent with larger effective population sizes over recent timescales [22]. In contrast,

298 IBnr had significantly lower $D_{SMP}$ compared to CEU (Figure 3B). This could be due to variation
299 in methylation rates, purifying selection, or demographic and selective (purifying selection)
300 histories. Therefore, we used SMCm [8], which employs fixed mutation rates and compares
301 the distributions of mutation and methylation markers, to estimate the forward and backward
302 methylation rates for the IBnr and CEU populations. Methylation rates were only slightly higher
303 in CEU but the ratio of backward to forward rates was similar in both populations (Figure S8).
304 Hypermutability should result in greater frequencies of intermediate variants [12], but we did
305 not observe such a pattern (Figure 2A). Tajima's *D* is based on a comparison of the number
306 of segregating sites versus π. The disparity in $D_{SMP}$ appears to be driven primarily by the
307 variation in the number of segregating sites per region (Figure S9). This difference suggests
308 that the demographic histories of the two populations may be slightly different.
309
310 We then estimated Tajima's *D* in different genomic contexts for CEU and IBnr. Clocklike
311 regions had significantly higher $D_{SNP}$ and $D_{SMP}$ compared to other regions (Figure 3B). The $D^m$
312 method assumes that forward and backward methylation rates are equivalent [28]. Although
313 the ratio of the backward to forward methylation rates in clocklike regions is 1.36, the ratios
314 are 2.11 and 2.84 for gbM and non-clocklike regions, respectively [10], indicating the
315 assumption of $D^m$ is less strongly violated for clocklike regions. $D_{SMP}$ for non-gbM regions was
316 slightly but significantly higher compared to the estimates for gbM regions (Figure 3B),
317 suggesting that ignoring the differences between regions can introduce minimal noise when
318 inferring evolutionary signatures from methylomes. The differences in $D_{SMP}$ between high-SIFT
319 vs low-SIFT were not consistent in both populations (Figure 3B). There was only a weak
320 positive correlation for π (Figure 3C) generated for SNPs vs SMPs that occur in coding regions
321 and no significant correlation for Tajima's *D* (Figure 3D).
322
323 We compared π and Tajima's *D* for *B. distachyon* SMPs generated using SNPs for the
324 Anatolian and Turkish lineage (B_East) [34, 35] to which all three clonal groups belong. Scaled
325 π for SMPs was larger for the *B. distachyon* clonal groups compared to the *A. thaliana*

326 populations, but there were no consistent differences between gbM and non-gbM regions or
327 among clonal groups (Figure 3A, 3E). Similar to *A. thaliana* (Figure 3A), scaled π for SMPs in
328 all three clonal groups was three orders of magnitude larger than the median SNP-based
329 scaled π (~$1.8\times10^{-6}$) for the B_East lineage [34, 35] (Figure 3E). Similar to *A. thaliana* (Figure
330 3B), $D_{SMP}$ in the three clonal groups was negative. $D_{SMP}$ was slightly but significantly larger in
331 non-gbM regions compared to gbM regions (Figure 3F). These negative values contrast with
332 the positive $D_{SNP}$ for genetic variants in the B_East lineage [34]. Unlike in *A. thaliana* (Figure
333 S9), this contrast cannot be attributed primarily to the differences in the number of segregating
334 sites (Figure S10), meaning that it cannot be explained solely by the extent of genotyping.
335 $D_{SMP}$ was lower for Group 1.1 compared to the other two groups (Figure 3F), which is
336 consistent with the higher frequency of rare alleles in this group (Figure 2B).
337
338 **Linkage disequilibrium quickly erodes for methylation variants**
339

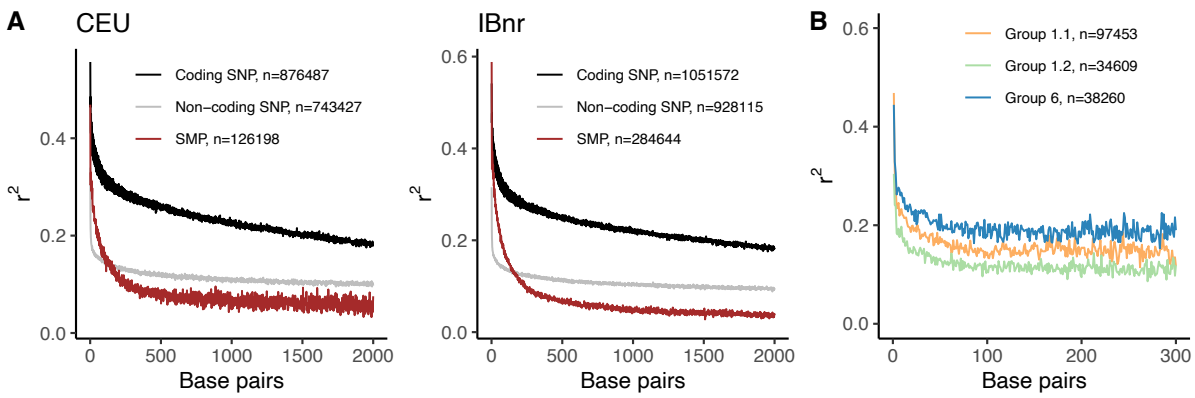


340
341 **Figure 4**. Weak linkage disequilibrium (LD) between neighboring single methylation
342 polymorphisms (SMP). (**A**) Pairwise $r^2$ estimated using coding single nucleotide
343 polymorphisms (SNP), non-coding SNPs, and SMPs for Central European (CEU) and Iberian
344 non-relicts (IBnr) *Arabidopsis thaliana* populations. The number of sites used for comparisons
345 is indicated within the plots. (**B**) Pairwise $r^2$ was estimated using SMPs for the clonal groups.
346 For (A) and (B), the number of sites used for comparisons is indicated within the plots.
347

348

349 An important consideration for population genetic analysis is the presence of sites with
350 independent evolutionary histories [8]. Therefore, we assessed the levels of pairwise linkage
351 disequilibrium (LD) to identify the number of independent polymorphic SNPs and SMPs.
352 Pairwise LD decay was stronger for noncoding SNPs compared to coding SNPs in *A. thaliana*
353 (Figure 4A). However, LD decay was much stronger for SMPs than for SNPs with $r^2$ dropping
354 below 0.1 within the first 250 bp (Figure 4A). LD decays to 0.1-0.25 for SMPs sites within gbM
355 regions for *B. distachyon* within the first 100 bp but remains constant thereafter (Figure 4B)
356 and is stronger compared to LD in *A. thaliana* over large distances (Figure 4A).

357

358 **Demographic inference using genetic and methylation variants**

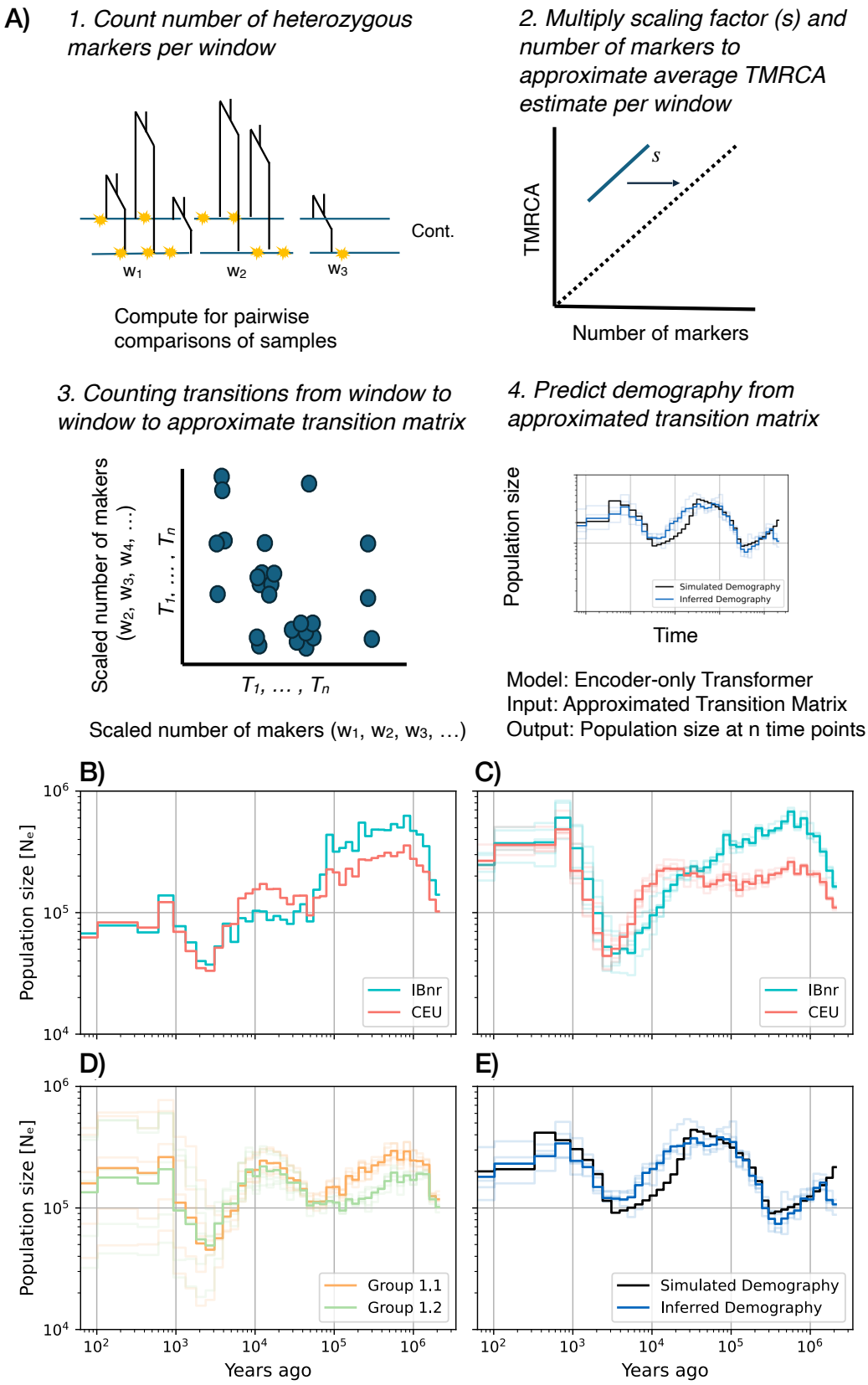


**Figure 5.** Demographic inference using mutation or methylation markers. **(A)** Schematic of the approximated transition matrix inference framework. The genome is first divided into 20

362 Kbp bins, and heterozygous markers are counted for all pairwise comparisons in a sample of
363 10 individuals. These counts are then scaled by an empirically chosen factor to ensure
364 sufficient values in the approximated transition matrix by aligning the number of markers per
365 window to the TMRCA in that window. The framework constructs this matrix by concatenating
366 all pairwise comparisons into a long sequence and applying a sliding window of size 2 and
367 step size 1. Each pair of consecutive values in this window represents coordinates in the
368 transition matrix, which is incremented at those positions. This process results in an
369 unnormalized transition matrix that captures the genetic relationships between samples.
370 Finally, an encoder-only transformer neural network takes this noisy matrix as input, implicitly
371 learning the fixed scaling factor, and predicts population sizes at various time points. Inference
372 using over 42 time steps using (**B**) single nucleotide polymorphisms (SNP) and (**C**) single
373 methylation polymorphisms (SMP) for the central European (CEU) and the Iberian non-relicts
374 (IBnr) *Arabidopsis thaliana* populations. (**D**) Demographic inference using SMP for Groups 1.1
375 and 1.2 of *Brachypodium distachyon*. SMP inference was done using sequences from all five
376 chromosomes (light lines, average in bold), while SNP inference is based on chromosome
377 one. (**E**) Inference of simulated sawtooth demography using five replicates, 4Mbp segments,
378 and 10 samples.
379
380
381 We developed a novel inference method that focuses on large genome blocks (20 Kbp
382 windows) likely spanning multiple coalescent genealogies (Figure 5A), to estimate the times
383 to the most recent common ancestor (TMRCA). Our method assumes that the number of
384 heterozygous markers per window is correlated with the average TMRCA. Essentially, longer
385 coalescent times allow more mutations and epimutations to accumulate. To mitigate the
386 possibility that older genealogies (long TMRCA) can be unexpectedly short due to immediate
387 recombination, our approach uses 20 Kbp windows to average out genealogies. We apply a
388 scaling to the number of markers to estimate the TMRCA (Figure S11). Although the chosen
389 scaling factor will not perfectly offset all variable demographic samples—given that we trained

using a fixed recombination rate and a fixed window size—offsets are minimal and addressed during training. An encoder-only transformer neural network processes this data, learns the scaling factor, and predicts population sizes over time. This is done by summarizing the TMRCA of two consecutive windows in the empirical transition matrix. The differences between each pair of samples are used to infer their TMRCA. The TMRCA values for all pairs across multiple intervals (windows) in the genome are then represented as a transition matrix. This method combines raw genotype data restructuring with deep learning to infer demographic history.

For deep learning inference, the distributions of heterozygous markers in training and real data must overlap to ensure in-distribution inference. For the training data, we collapsed each training transition matrix into a single scalar by summing the flattened matrix and plotted the distribution of unnormalized transition matrices (Figure S12A). To ensure the real data *from A. thaliana* and *B. distachyon* matched the training data, we analyzed 20 randomly sampled genomic regions. For the SNP data, we selected start positions uniformly between 0-28 Mbp, whereas for the methylation data, the start positions were chosen uniformly between 0-0.5 Mbp. For both data types, we determined each region's length by sampling from a uniform distribution between 1-3 Mbp. Summing the resulting transition matrices for the IBnr, CEU, Group 1.1, and Group 1.2 regions (Figure S12B-D) produced values within the training data range (Figure S12A). Despite the differential properties of SMPs and SNPs, the distribution of heterozygous markers per 20 Kbp window was similar across populations (Figure S12B-C), supporting the use of a common training dataset for deep learning.

We applied our coarse−grained inference approach to *A. thaliana* and *B. distachyon*. We generated approximated transition matrices from 10 samples and 4 Mbp sequence lengths. The 45 pairwise comparisons totaling 180 Mbp with 20 Kbp windows yielded 9,000 pairs of TMRCA values per matrix. We detected a population bottleneck ~100,000 years ago (100 kya) in CEU and IBnr using SNPs (Figure 5B), which was consistent with the findings of a previous

418 study [22]. This signal was not clearly detected with SMPs (Figure 5C), indicating their limited
419 use for ancient events. Both SNPs and SMPs indicated another bottleneck between 1-10 kya
420 (Figure 5B-C), but SMPs also revealed a subsequent population expansion (Figure 5C)
421 undetected by SNPs (Figure 5B). The population contraction began earlier in IBnr, followed
422 by a slightly stronger expansion compared to CEU (Figure 5C), which may explain its more
423 negative Tajima's *D* estimate for methylation variants (Figure 3B). Using SMPs, we recovered
424 two bottlenecks (~100 kya and between 1-10 kya) in *B. distachyon* (Figure 5D) that were
425 previously reported using SNPs for samples combined from multiple clonal groups in this
426 species [34]. The steeper expansion of IBnr compared to CEU (*A. thaliana*) and Group 1.1
427 compared to Group 1.2 (*B. distachyon*) in the last 10,000 years likely led to the observed
428 excess of rare alleles (Figures 2B, 3F).
429
430 We validated our demographic inference with two approaches. First, we simulated the
431 sawtooth demography observed in both species, confirming that our deep learning method
432 accurately detected multiple bottleneck and expansion events (Figure 5E). Second, we
433 simulated methylation markers with high rates of change ($10^{-4}$, $10^{-5}$, or $10^{-6}$ per site per
434 generation) and backward rates 2.5 times larger than forward rates, based on the estimates
435 provided in [6], to test whether deviations from the infinite sites model affect inference. We
436 found that our method accurately recovered demographic histories beyond 0.6 kya and before
437 5, 22, and 442 kya for methylation rates of $10^{-4}$, $10^{-5}$, and $10^{-6}$ per site per generation,
438 respectively (Figure S13). Conservatively, this suggests that inferences 20 kya and beyond
439 are unlikely to be accurate for CEU and IBnr due to their estimated rates of methylation change
440 being around $10^{-5}$ per site per generation (Figure S8). Note that the demographic estimates
441 with SNPs are likely accurate for older events (>20kya). Nonetheless, we are confidently
442 estimating recent population expansion with SMPs (Figure 5C), highlighting the potential of
443 methylation markers to reveal insights beyond what genetic variants alone can provide.
444
445

446 **Discussion**

447 We observed contrasting patterns in the capacity of methylation variants to distinguish
448 population subdivisions in *A. thaliana* and *B. distachyon*. In *A. thaliana*, the infinite sites model
449 is likely violated for methylation, resulting in the erosion of methylome differentiation likely due
450 to the older divergence between populations. In *B. distachyon*, samples from different altitudes
451 with varying seed morphologies exhibited distinct methylation profiles in a common garden,
452 despite their genetic similarity. While SMP distributions are similar across different genomic
453 contexts, DMRs are more context dependent, making the former preferable for population-
454 scale analyses. We found weak negative correlations between π and no local correlations for
455 Tajima's *D* between genetic variants and methylation variants in *A. thaliana*, underscoring their
456 distinct molecular and evolutionary properties, similar to the conclusions reached by Schmitz
457 *et al.* (2013) [36]. We found slightly stronger linkage between neighboring SMPs compared to
458 a previous estimate in wild *A. thaliana* sampled across the Northern Hemisphere [36], likely
459 due to our focus on individual populations with less genetic structure [22]. SMPs and SNPs
460 recover recent and older demographic changes, respectively, providing a comprehensive
461 reconstruction of population evolutionary histories.

462

463 The differing ability to detect population subdivisions in *A. thaliana* and *B. distachyon* using
464 methylation variants could lead to differences in divergence times, methylation rates, or local
465 adaptation. As the post-glacial re-colonization of the Iberian Peninsula and the spread
466 northward started ~16 kya [29], multiple changes at the same methylation site (homoplasy)
467 during this period may have caused an underestimation of the true levels of divergence in *A.*
468 *thaliana*. The greater capacity to detect group subdivision is *B. distachyon* could reflect a
469 recent separation by altitude contributing to methylome divergence. We indeed rule out the
470 role of adaptation such as found in *F. vesca* [17], because we generated inferences using gbM
471 regions that are highly conserved in angiosperms [11]. The observed divergence could be due
472 to low rates of methylation change, but we could not estimate methylation rates for *B.*
473 *distachyon* as our rate estimate relies on comparing the distributions of genetic and

474 methylation variants. The most parsimonious explanation is that the two subgroups diverged
475 recently. As the B_East lineage split from the western Mediterranean lineage 23 kya [34, 35],
476 the split between the closely related subgroups is likely to have been far more recent, ensuring
477 that the infinite sites model was not violated for methylation variants. Our findings underscore
478 the necessity for methods distinguishing neutral demographic changes from selective
479 pressures on the methylome, elucidating why SMPs behave differently across species.
480
481 Our results support the use of individual CG sites from all genomic contexts for population-
482 scale analyses. Our between-population comparisons using CG sites in gbM regions
483 successfully identified the known population structure within *B. distachyon*, similar to a
484 previous study using genic CG sites [16]. Further supporting this conclusion is the consistent
485 similarity in the mSFS shape when using SMPs, regardless of their genomic context. The *A.*
486 *thaliana* [21] and *B. distachyon* [16] methylomes, generated under similar environmental
487 conditions, ensure that sites affected solely by transient environmental effects would not be
488 recognized as SMPs. Another study using all CG sites from lettuce methylomes, cultivated
489 under uniform environmental conditions, also demonstrated the capacity to distinguish
490 multiple species [19]. Some noise can be introduced by analyzing the whole methylome as
491 non-gbM regions show a slight skew towards variants with intermediate frequencies, but this
492 is likely to be offset by the increased number of sites for inference. The distribution of DMR
493 states is tied to the genomic context. gbM results from the combined activity of MET1, which
494 is enhanced by nearby existing methylation, as well as the histone variant H2A.Z and the DNA
495 demethylase ROS1 [37]. The molecular basis underlying the clock-like, non-gbM regions, as
496 well as regions with high and low SIFT scores, remains unknown. However, given that our
497 mSFS for these regions differ, this suggests potential for differences in their molecular basis.
498 Studying DMRs can nevertheless be valuable for imputing methylation states when
499 sequencing depths are low [38], while the impact of such imputation on population genetics
500 inference needs to be evaluated. Overall, using a restricted set of CG sites may be more

501 appropriate when analyzing accessions grown under variable environments together or for
502 tracking long-term methylome divergence [10].
503
504 The weak local correlations between genetic and methylation diversity and the association
505 between gene constraint and methylation diversity in *A. thaliana* can partly be attributed to
506 methylation affecting the mutability of neighboring sites [39-41] and transposable element
507 polymorphisms influencing methylation variation [42, 43]. However, only about 12% of
508 methylation quantitative trait loci (QTLs) in *A. thaliana* are within 10Kbp of the epiallelic target
509 [36]. In maize, approximately 50% of methylation QTLs occur in *cis* [44], indicating a potentially
510 stronger trend in this species. The higher rate of methylation changes compared to mutation
511 accumulation [6, 7] may also explain why methylation differences persist despite genetic
512 homogeneity. Our simulations also show that coalescent histories of markers with vastly
513 different rates of change diverge, which can explain the general lack of correlation between π
514 and Tajima's *D* for local genetic and methylation diversity. Our results are similar to those of
515 previous studies in lettuce [19] and cotton [45], which also found higher levels of polymorphism
516 in the methylome compared to the genome. The lack of correlation or similarity between the
517 Tajima's *D* estimates from the genome and methylome in *A. thaliana* and *B. distachyon*
518 supports the notion that the SNPs and SMPs likely reflect different parts of the common
519 underlying coalescent genealogy at a locus: SNPs reflect the older part of the tree, whereas
520 SMPs would reflect the topology and branch lengths in the more recent past. It is then not
521 surprising that for recent positive selection events (selective sweeps), the signatures are
522 similar for both types of markers, and SMPs may even be more accurate in detecting them
523 [15]. Our study mostly focuses on local correlations in diversity, rather than genome-wide
524 correlations, where life history traits and genetic differentiation levels also play a significant
525 role [46-52].
526
527 Our study demonstrates that methylation variants can independently detect and allow
528 inference of historical demographic changes. This represents a significant improvement over

529 a previous approach [8], where methylation was used only as a secondary marker to
530 supplement genetic variant-based inferences. Furthermore, our improved deep learning
531 method does not require precise methylation rate parameters and is less sensitive to the
532 presence of invariant methylation sites (compared to the SMCm in [8]). Instead, it trains on
533 diverse scenarios to match observed variant distributions. For *B. distachyon*, methylation
534 variants revealed expansions also detected by genetic variants [34]. In *A. thaliana*, genetic
535 variant-based demographic inferences fail to detect recent population expansions (this study
536 and [53]), which can be uncovered through methylation variants instead. Our simulations
537 confirmed the utility of rapidly mutating markers for inferring demographic changes. Overall,
538 our study highlights the value of methylation markers for understanding recent shifts in
539 population size.
540
541
542 **Conclusions**
543 Our findings demonstrate that CG methylation can provide new insights into population
544 structure in clonal and selfing species, similar to its previously demonstrated utility in *A.*
545 *thaliana* from America and the clonal seagrass *Zostera marina* [10]. We demonstrate the utility
546 of methylation variants for uncovering very recent demographic events, where SNP markers
547 are limited due to their slower rate of change. We also illustrate its usefulness in clonal groups,
548 where the paucity of SNPs would render such inferences either impossible or necessitate very
549 deep and costly levels of DNA sequencing. Conversely, at older timescales, methylation
550 markers are unlikely to be informative because the high rates of change would have resulted
551 in the violation of the infinite sites model. We show that SNPs and SMPs are complementary
552 for generating demographic inferences over short and long timescales, highlighting the value
553 of a recently developed method that leverages both sources of variation for inferring
554 demography [8]. Our work demonstrates that methylomes contain unique evolutionary insights
555 unattainable through studying genomic variation in isolation.
556

557

558 **Methods**

559 *Genetic and methylation variant calling in Arabidopsis thaliana*

560 We obtained the *A. thaliana* 1001 genomes [30] SNP calls from
561 https://1001genomes.org/data/GMI-MPI/releases/v3.1/. We only retained biallelic SNPs for
562 our analyses. As C/T variant calls can become confounded with methylation calls for data
563 generated using bisulfite sequencing, we generated sample-specific genome references for
564 mapping bisulfite sequencing reads. We substituted the genetic variant calls for each sample
565 into the TAIR10 genome reference [54] using SAMtools [55], BCFtools consensus [55], and
566 fastq split [56]. We obtained bisulfite sequencing data for the 1001 *A. thaliana* from [21]. We
567 first removed poor-quality reads using Trimmomatic [57] with the following options:
568 ILLUMINACLIP:TruSeq3-SE.fa:2:30:10 LEADING:3 TRAILING:3 SLIDINGWINDOW:4:15
569 MINLEN:36 for single-end reads and ILLUMINACLIP:TruSeq3-PE.fa:2:30:10:2:True
570 LEADING:3 TRAILING:3 SLIDINGWINDOW:4:20 MINLEN:36 for paired-end reads. We
571 subsequently mapped reads to the sample-specific reference genomes using Bismark with
572 the aid of the HISAT2 aligner [58]. We ran Bismark deduplicate_bismark to remove optical
573 duplicates and ran bismark_methylation_extractor to extract methylation calls. We studied
574 cytosine sites with a coverage of at least five reads similar to what was done in [21]. To identify
575 the methylation state of a site, we performed a binomial test with the non-conversion rate being
576 used as the hypothesized probability of success following the method in [59]. The non-
577 conversion rate was calculated as the proportion of methylation in the chloroplast as done in
578 [59]. Sites were assigned as methylated if the false discovery rate corrected *P*-values following
579 the binomial test was less than 0.01. Otherwise, they were designated as unmethylated. We
580 used jDMR [60] to identify DMRs in the CG contexts as this method accounts for coverage
581 when calculating likelihood scores for methylation states. For this, we called the methylation
582 status per site using METHimpute (function: callMethylationSeparate) [38], extracted cytosine
583 clusters in the CG context ensuring that there was a minimum of eight cytosines in each cluster
584 (function: CfromFASTAv4 and makeReg with default options makeRegnull = c(FALSE), N.boot

585 = 10^5, N.sim.C = "all", fp.rate = 0.01, set.tol = 0.01), and identified the methylation states of
586 the regions in each sample (function: runMethimputeRegions), ensuring that we used a
587 minimum of eight cytosines and a coverage of three.
588
589 63 IBnr and 67 CEU samples overlapped between the SNP and methylation variant call files.
590 We randomly subsampled 63 samples from the CEU population to ensure the numbers were
591 comparable to those of the IBnr population. For our analyses, we only used sites where at
592 least 80% of the samples within each population were genotyped. The proportions of variant
593 SNP and SMP sites were calculated by dividing the number of sites with minor allele
594 frequencies greater than 0.02 by the total number of variant and invariant sites.
595
596 *Population (epi)genetic metric estimation for Arabidopsis thaliana*
597 To estimate π and Tajima's *D*, we created fasta files for each genomic region containing the
598 sequences for each sample. We substituted the variants from the SNP vcf into the TAIR10
599 reference genome using the approach described previously for each sample, extracted the
600 region of interest, and converted it to a fasta format. The regions could be the clocklike regions
601 described in [10], genic regions comprising all exons, or non-coding regions comprising all
602 regions other than exons. Genic regions were further split into gbM genes using the list for *A.*
603 *thaliana* provided by [61] and high SIFT-score (>0.75) and low SIFT-score (<0.3) genes using
604 the list provided by [62].
605
606 We estimated $\pi_{SNP}$ and $D_{SMP}$ using pegas [63] and estimated $\pi_{SMP}$ and $D_{SMP}$ using the $D^m$ [28].
607 We only analyzed intervals that had at least three polymorphic sites and sequences with
608 lengths greater than 10bp. We calculated the number of cytosines in each interval using
609 METHimpute [38]. To compare π and Tajima's *D* among the different genomic contexts, we
610 built a linear model where these metrics were the dependent variable, and the concatenated
611 population and genomic context groupings were the predictor variables. We then applied a
612 Tukey honest significant differences test using the agricolae R package

613 (https://myaseen208.com/agricolae//index.html) to identify significant differences between
614 individual predictor levels. We performed a correlation test to compare the π and Tajima's *D*
615 for SMPs and SNPs per exon.
616
617 We used VCFtools [64] to estimate the allele frequencies for SMPs and DMRs. We used
618 PopLDdecay [65] to estimate pairwise LD using the $r^2$ metric analyzing all sites with a minor
619 allele frequency greater than 0.005.
620
621 *Between population comparisons for Arabidopsis thaliana*
622 We combined the CEU and IBnr vcfs and used VCF2Dis (https://github.com/BGI-
623 shenzhen/VCF2Dis) to estimate the p-distance matrix. We used this matrix to generate
624 neighbor-joining trees using FastME [66] and plotted it using ggtree [67]. We also performed
625 DAPC to discriminate samples from the CEU and IBnr populations. We thinned the dataset so
626 that only sites that were separated by 1Kbp were sampled to reduce the computational time.
627 We converted vcf files into a genlight format using the *genomic_converter* function in the R
628 package radiator (https://thierrygosselin.github.io/radiator/). We used the find.clusters function
629 in adegenet [68] to identify the number of clusters in each dataset allowing for a maximum of
630 20 clusters for SMPs/DMRs and 30 clusters for SNPs. As DAPC regions require fully typed
631 data, we imputed missing values using the mean value. Then, we performed cross-validation
632 using adegenet [68] to identify the number of informative principal components. We retained
633 a maximum of 15 principal components, used 90% of the data for training, and calculated
634 group-wise assignment success. We centered but did not scale variables. We used 30
635 replicates for each principal component. Finally, we performed DAPC using adegenet [68].
636
637 Methylation rate estimation *for Arabidopsis thaliana*
638 We generated the multihetsep files for SNPs for the same 5Mbp regions that were used for
639 SMPs (described in the section immediately above). We combined the SNP and SMP
640 multihetsep files. We randomly selected 20 samples from each population to ensure

641 reasonable runtimes. We used the *Methylation_rate_estimation* function in SMCm to estimate
642 forward and backward rates [8]. We set the mutation rate as $7\times10^{-9}$ per site per generation
643 and the recombination rate as $3.5\times10^{-8}$ per site per generation. We ignored regional influences
644 on methylation rates and estimated rates under a site-only model. We used the known
645 estimates of forward ($2.56\times10^{-4}$ per generation per haploid methylome) and backward
646 methylation rates ($6.3\times10^{-4}$ per generation per haploid methylome) for *A. thaliana* [6] as
647 priors.
648
649 *Genetic and methylation variant calling in Brachypodium distachyon*
650 We obtained whole genome sequencing data (29 samples) for *B. distachyon* from [27] and
651 whole genome bisulfite sequencing data from [16]. We used Bd21-3 v1.2 genome reference
652 and the GenBank annotation from the Joint Genome Institute (http://phytozome.jgi.doe.gov/)
653 for variant calling. We used Trimmomatic [57] to trim reads using the paired-end options as
654 stated above for the whole genome sequencing data and the single-end option for the whole
655 genome bisulfite sequencing data. We mapped whole genome sequencing data reads to the
656 reference using bwa-mem [69]. We used Picard Toolkit (https://broadinstitute.github.io/picard/)
657 to add read groups and mark duplicate reads. We used SAMtools [55] to remove unpaired
658 reads, remove reads with a mapping quality of less than 20, and sort reads. We called genetic
659 variants using GATK HaplotypeCaller [70]. We only retained SNPs with depths greater than
660 five and quality scores greater than 30 using BCFtools [55]. Using this SNP variant call file,
661 we perform methylation variant calling in the same way as was done for *A. thaliana*. We
662 obtained the sample localities from [32] and created a map showing their occurrence with Map
663 Maker (https://maps.co/).
664
665 *Within and between population analyses in Brachypodium distachyon*
666 We used a minor allele frequency threshold of 10% to identity polymorphic sites in each clonal
667 group due to the smaller number of samples being analyzed when compared to *A. thaliana*.
668 For the analysis of SMPs and DMRs, we only used variants that occurred within CG-gbM

regions identified in [71]. We estimated mSFS, LD, p-distance matrices, π, and Tajima's *D* in a similar way as we did for *A. thaliana*. We thinned the SMP dataset so that only sites that were separated by 3Kbp were sampled to reduce the computational time for the DAPC analyses.

*Generating the approximated transition matrix for demographic inference*

We created a training and testing dataset consisting of a combined $60\times10^3$ simulations (80%/20%, respectively). Of these $10\times10^3$ were constant demographies (*i.e.*, no demographic change) with a random population size drawn between $10\times10^3$ and $200\times10^3$, and the other $50\times10^3$ simulations were random walk demographies, with time steps being defined for i ∈ {0,1,...,K − 1} using:

$$(\text{population_time})_i = \frac{\exp\left(\frac{i}{K-1}\cdot\ln(1+\delta t_{\text{max}})\right)-1}{\delta}$$

where $K$=42 is the number of time points, $\delta$ = 0.001 is the growth rate, and $t_{\text{max}} = 2.1\times10^6$ is the maximum time.

The population size was drawn for each of the $K$=42 time points in the following way: an initial population size was randomly selected between a minimum (*N_min* = $10\times10^3$) and maximum (*N_max* = $1.2\times10^6$) value. For each subsequent time point, a new population size was proposed by multiplying the previous size by a random factor between 0.1 and 10. If this proposed size fell outside the allowed range (N_*min* to *N_max*), new proposals were generated until an acceptable value was found. This process was repeated for all 42 time points, resulting in a sequence of population sizes that exhibit both gradual and abrupt changes while remaining within the specified bounds. Nevertheless, a sliding window average with a size of 6 and a step size of 1 was applied to smooth extreme changes. This approach for sampling demographies was adapted from Sanchez *et al*. [72].

The obtained population sizes and times were passed onto *msprime* [73] to simulate the corresponding ancestral recombination graphs using a recombination rate of $3.4\times10^{-8}$ per base pair and generation. For SNPs, branches were mutated at a rate of $7\times10^{-9}$ per base pair and generation, leading to a $\rho$ over $\theta$ ratio of 4.86.

Simulated and real data are summarized as a genotype matrix (*GM*) with dimensions $n \times m$, where $n,m \in \mathbb{N}$ represent the number of samples and mutations, respectively. Each element $g_{ij}$ of *GM*, where $i \in \{1,...,n\}$ and $j \in \{1,...,m\}$, denotes the presence ($g_{ij} = 1$) or absence ($g_{ij} = 0$) of mutation *j* in sample *i*. We generated a corresponding vector of positions of size *m* for each segregating site containing floating point numbers of the location in the genome.

For each random population size parameter, we used a genome of length 4Mbp,10 samples (ploidy=1), and the *GM* and positions vector to construct a density estimate of mutations along the genome (in theory, corresponding to the respective TMRCA at that region). To ensure the presence of enough markers, we segmented the genome into 20Kbp pieces and counted the number of heterozygous markers between all pairwise $\binom{10}{2}$ combinations. The 4Mbp sequences of all the comparisons were concatenated and log-transformed. Likewise, the population time steps were also log-scaled. To make sure that the number of markers per window fell approximately into the time windows, we scaled the markers by an arbitrarily

chosen scaling factor (=$e^{8.2}$) (Figure S13). The importance of the given scaling factor is negligible, due to all the transformation steps occurring in the pre-training, and therefore any noisy representation presented to the learning algorithm will be part of the training.

Each *msprime* simulation (under a random demographic history) yielded one *approximated* transition matrix, which was obtained by counting the transitions (scaled number of heterozygous sites in window t → window t+1) from one 20 Kbp window to the next using the following algorithm: a sliding window of size 2 and step size 1 was applied along the sequence and each pair of consecutive values in this window represents coordinates in the transition matrix, which was incremented at those positions leading to a filled matrix which remained unnormalized. Lastly, the entire transition matrix was incremented by one at each entry and scaled by the natural log to squeeze all values approximately into the same range to avoid training instability.

*Model description, training, and inference*

The inference approach can be described as a supervised learning approach using the *approximated* transition matrices *x* with defined dimensions $R^{L=42\times K=42}$ as the input and the population size at each time step as the predicted variable. The input is a square matrix where both dimensions (K and L) are 42. The model architecture is an encoder-only transformer [74] (https://github.com/lucidrains/x-transformers). It consists of three main components: an input projection layer, a transformer encoder, and an output projection layer. It can be formalized as:

1. Input Projection: $x_{proj} = W_{in}x + b_{in}$, where $W_{in} \in R^{D_{enc}\times K_{in}}, b_{in} \in R^{D_{enc}}, x \in R^{L\times K_{in}}$
2. Transformer Encoder: $z = \text{Encoder}(x_{proj})$, where $z \in R^{L\times D_{enc}}$

742 The Encoder employs a configuration with dimension $D_{enc}$ = 512, depth $N_{enc}$ = 12, number
743 of attention heads $H_{enc}$ = 10 heads, Gated Linear Unit activation in feed-forward layers [75],
744 residual attention connections [76], and rotary positional embeddings [77].
745 3. Dimension Reduction: $z_{reduced} = \sum_{i=1}^{L} z_i$ , where $z_{reduced} \in R^{D_{enc}}$
746 4. Output Projection: $y = W_{out} z_{reduced} + b_{out}$, where $W_{out} \in R^{D_{out} \times D_{enc}}, b_{out} \in R^{D_{out}}$
747
748 In this formalization, sequence length $L$ = the input dimension of the transition matrix $K_{in}$ =
749 42, which represents the square input matrix of 42 x 42 dimensions, and the output
750 dimension $D_{out}$ = 42.
751
752 The neural network model underwent training for 50 epochs, employing mean squared error
753 as the loss function. The training process leverages the Accelerate framework from Hugging
754 Face to enhance performance [78]. An Accelerator object was configured with mixed precision
755 using bfloat16 and gradient accumulation over 12 steps (with batch size 32). Throughout the
756 training regiment, both the training and test losses were continuously monitored to evaluate
757 model performance and assess convergence.
758
759 *Generating data for demographic inference*
760 We first generated unique variant call files for each sample from the population variant call
761 files using BCFtools [55]. We then used the generate_multihetsep.py from MSMC-tools
762 (https://github.com/stschiff/msmc-tools/tree/master) to combine all the samples per
763 chromosome. For *A. thaliana* SNPs, we used the entire chromosome 1 as we needed a long
764 contiguous fragment to generate the approximated transition matrix. For SMPs, we used 5Mbp
765 segments in each of the five chromosomes (Table S2) as the SMP density was far higher. We
766 used the list of genotyped cytosine positions as a genomic location mask for the SMPs. For
767 *B. distachyon*, we included singletons to support the demographic inference given the small
768 sample sizes in this species. The data were polarized by identifying the minor (less frequent)

alleles and encoding them as derived, whereas the major alleles were encoded as ancestral. The resulting genotype matrix represents this polarized, unphased data, where each row corresponds to an individual and each column corresponds to a genomic position.

*Methylation simulation model*

We explored the boundaries of our course-grained demographic inference by adding a new mutation model to msprime [73]. We simulated a sawtooth demographic model with cyclical population size changes over time and a baseline effective population size of $2\times10^5$ individuals. Simulations were conducted on a 5Mbp sequence with a recombination rate of $3.4\times10^{-8}$ per base pair per generation (ploidy=1), to isolate the influence of methylation dynamics.

A custom matrix mutation simulation was implemented to model methylation and demethylation processes, employing 2 allelic states: 0 (unmethylated) and 1 (methylated). The model incorporates 3 key rates: the site introduction rate ($\mu$), methylation rate ($\beta$), and demethylation rate ($\delta$). The methylation and demethylation rates are measured as factors of the site entry rate, where $\beta$ = the methylation factor$\cdot\mu$ and $\delta$ = the demethylation factor$\cdot\mu$. The transition probabilities between the unmethylated and methylated states are determined by the ratio $\beta/(\beta+\delta)$ for methylation and $\delta/(\beta+\delta)$ for demethylation. The resulting 2×2 transition matrix encapsulates these probabilities:

$$\begin{bmatrix} 1 - [\beta/(\beta+\delta)] & \beta/(\beta+\delta) \\ \delta/(\beta+\delta) & 1 - [\delta/(\beta+\delta)] \end{bmatrix}$$

This framework allowed us to explore various methylation scenarios by adjusting $\beta$ and $\delta$ relative to $\mu$. We investigated cases where $\beta = \mu$ and $\delta = 2.5\mu$, $\beta = 10\mu$ and $\delta = 25\mu$, and $\beta = 100\mu$ and $\delta = 250\mu$, representing low, medium, and high methylation dynamics respectively, with the demethylation rate 2.5 times higher than the methylation rate. By varying the

epimutation rate compared to the mutation rate, we test the robustness of our approach in correlating the number of markers in one Kbp windows with the average coalescent time. This proportionality, and the robustness of our method, is expected to decrease for higher epimutation rates, as these would violate the infinite site model for older coalescent times more strongly (due to homoplasy, [4]).

## Declarations

*Ethics approval and consent to participate*

Not applicable

*Consent for publication*

Not applicable

*Availability of data and materials*

The scripts for analyzing and plotting all the results, except for the demographic inference, have been published on GitHub (arunkumarramesh/methevolve) and archived using Zenodo (https://doi.org/10.5281/zenodo.13991812). The demographic inference method is available on GitHub (kevinkorfmann/aTMi) and has been archived using Zenodo (https://doi.org/10.5281/zenodo.13332833).

*Competing interests*

The authors declare that they have no competing interests.

*Funding*

RA was funded by the Peter and Traudl Engelhorn Foundation.

*Authors' contributions*

RA and AT designed the research. RA, KK, AW, BH, CG, and YW performed the research. RA, AT, KK, and AW wrote the paper. All authors read and approved the final manuscript.

*Acknowledgements*

We would like to thank Thibaut Paul Patrick Sellinger for helping with the estimation of methylation rates. This work was supported by the de.NBI Cloud within the German Network for Bioinformatics Infrastructure (de.NBI) and ELIXIR-DE (Forschungszentrum Jülich and W-de.NBI-001, W-de.NBI-004, W-de.NBI-008, W-de.NBI-010, W-de.NBI-013, W-de.NBI-014, W-de.NBI-016, W-de.NBI-022).

**References**

1. Richards CL, Alonso C, Becker C, Bossdorf O, Bucher E, Colome-Tatche M, Durka W, Engelhardt J, Gaspar B, Gogol-Doring A, et al: **Ecological plant epigenetics: Evidence from model and non-model species, and the way forward.** *Ecol Lett* 2017, **20:**1576-1590.
2. Feng S, Cokus SJ, Zhang X, Chen PY, Bostick M, Goll MG, Hetzel J, Jain J, Strauss SH, Halpern ME, et al: **Conservation and divergence of methylation patterning in plants and animals.** *Proc Natl Acad Sci U S A* 2010, **107:**8689-8694.
3. Zhang H, Lang Z, Zhu JK: **Dynamics and function of DNA methylation in plants.** *Nat Rev Mol Cell Biol* 2018, **19:**489-506.
4. Vidalis A, Zivkovic D, Wardenaar R, Roquis D, Tellier A, Johannes F: **Methylome evolution in plants.** *Genome Biol* 2016, **17:**264.
5. Cortijo S, Wardenaar R, Colome-Tatche M, Gilly A, Etcheverry M, Labadie K, Caillieux E, Hospital F, Aury JM, Wincker P, et al: **Mapping the epigenetic basis of complex traits.** *Science* 2014, **343:**1145-1148.

848 6. van der Graaf A, Wardenaar R, Neumann DA, Taudt A, Shaw RG, Jansen RC,
849 Schmitz RJ, Colome-Tatche M, Johannes F: **Rate, spectrum, and evolutionary**
850 **dynamics of spontaneous epimutations.** *Proc Natl Acad Sci U S A* 2015,
851 **112:**6676-6681.
852 7. Ossowski S, Schneeberger K, Lucas-Lledo JI, Warthmann N, Clark RM, Shaw RG,
853 Weigel D, Lynch M: **The rate and molecular spectrum of spontaneous**
854 **mutations in Arabidopsis thaliana.** *Science* 2010, **327:**92-94.
855 8. Sellinger T, Johannes F, Tellier A: **Improved inference of population histories by**
856 **integrating genomic and epigenomic data.** *eLife* 2023, **12:**RP89470.
857 9. Yao N, Schmitz RJ, Johannes F: **Epimutations Define a Fast-Ticking Molecular**
858 **Clock in Plants.** *Trends Genet* 2021, **37:**699-710.
859 10. Yao N, Zhang Z, Yu L, Hazarika R, Yu C, Jang H, Smith LM, Ton J, Liu L, Stachowicz
860 JJ, et al: **An evolutionary epigenetic clock in plants.** *Science* 2023, **381:**1440-
861 1445.
862 11. Muyle AM, Seymour DK, Lv Y, Huettel B, Gaut BS: **Gene Body Methylation in**
863 **Plants: Mechanisms, Functions, and Important Implications for**
864 **Understanding Evolutionary Processes.** *Genome Biol Evol* 2022, **14:**evac038.
865 12. Charlesworth B, Jain K: **Purifying selection, drift, and reversible mutation with**
866 **arbitrarily high mutation rates.** *Genetics* 2014, **198:**1587-1602.
867 13. Muyle A, Ross-Ibarra J, Seymour DK, Gaut BS: **Gene body methylation is under**
868 **selection in Arabidopsis thaliana.** *Genetics* 2021, **218:**iyab061.
869 14. Xu G, Lyu J, Li Q, Liu H, Wang D, Zhang M, Springer NM, Ross-Ibarra J, Yang J:
870 **Evolutionary and functional genomics of DNA methylation in maize**
871 **domestication and improvement.** *Nat Commun* 2020, **11:**5539.

872 15. Shirai K, Sato MP, Nishi R, Seki M, Suzuki Y, Hanada K: **Positive selective**
873 **sweeps of epigenetic mutations regulating specialized metabolites in**
874 **plants.** *Genome Res* 2021, **31:**1060-1068.
875 16. Eichten SR, Srivastava A, Reddiex AJ, Ganguly DR, Heussler A, Streich JC, Wilson
876 PB, Borevitz JO: **Extending the Genotype in Brachypodium by Including DNA**
877 **Methylation Reveals a Joint Contribution with Genetics on Adaptive Traits.**
878 *G3 (Bethesda)* 2020, **10:**1629-1637.
879 17. Le Vève A, Sammarco I, Latzel V, Lafon Placette C: **DNA methylation shows**
880 **footprints of altitude selection in the clonal plant species Fragaria vesca.**
881 *bioRxiv* 2024, **2024.03.19.585697**.
882 18. Sammarco I, Diez Rodriguez B, Galanti D, Nunn A, Becker C, Bossdorf O,
883 Munzbergova Z, Latzel V: **DNA methylation in the wild: epigenetic**
884 **transgenerational inheritance can mediate adaptation in clones of wild**
885 **strawberry (Fragaria vesca).** *New Phytol* 2024, **241:**1621-1635.
886 19. Cao S, Sawettalake N, Li P, Fan S, Shen L: **DNA methylation variations underlie**
887 **lettuce domestication and divergence.** *Genome Biol* 2024, **25:**158.
888 20. Rodriguez-Izquierdo A, Carrasco D, Anand L, Magnani R, Catarecha P, Arroyo-
889 Garcia R, Rodriguez Lopez CM: **Epigenetic differences between wild and**
890 **cultivated grapevines highlight the contribution of DNA methylation during**
891 **crop domestication.** *BMC Plant Biol* 2024, **24:**504.
892 21. Kawakatsu T, Huang SC, Jupe F, Sasaki E, Schmitz RJ, Urich MA, Castanon R,
893 Nery JR, Barragan C, He Y, et al: **Epigenomic Diversity in a Global Collection of**
894 **Arabidopsis thaliana Accessions.** *Cell* 2016, **166:**492-505.

22. Strütt S, Sellinger T, Glemin S, Tellier A, Laurent S: **Joint inference of evolutionary transitions to self-fertilization and demographic history using whole-genome sequences.** *Elife* 2023, **12:**e82384.

23. Vaswani A, Shazeer N, Parmar N, Uszkoreit J, Jones L, Gomez AN, Kaiser L, Polosukhin I: **Attention Is All You Need.** *arXiv* 2017, **1706.03762**.

24. Devlin J, Chang M-W, Lee K, Toutanova K: **BERT: Pre-training of Deep Bidirectional Transformers for Language Understanding.** *arXiv* 2018, **1810.04805**.

25. Korfmann K, Gaggiotti OE, Fumagalli M: **Deep Learning in Population Genetics.** *Genome Biol Evol* 2023, **15**.

26. Becker C, Hagmann J, Muller J, Koenig D, Stegle O, Borgwardt K, Weigel D: **Spontaneous epigenetic variation in the Arabidopsis thaliana methylome.** *Nature* 2011, **480:**245-249.

27. Wilson PB, Streich JC, Murray KD, Eichten SR, Cheng R, Aitken NC, Spokas K, Warthmann N, Gordon SP, Accession C, et al: **Global Diversity of the Brachypodium Species Complex as a Resource for Genome-Wide Association Studies Demonstrated for Agronomic Traits in Response to Climate.** *Genetics* 2019, **211:**317-331.

28. Wang J, Fan C: **A neutrality test for detecting selection on DNA methylation using single methylation polymorphism frequency spectrum.** *Genome Biol Evol* 2014, **7:**154-171.

29. Hewitt G: **Post-glacial re-colonization of European biota.** *Biological Journal of the Linnean Society* 1999, **68:**87-112.

30. The1001GenomesConsortium: **1,135 Genomes Reveal the Global Pattern of Polymorphism in Arabidopsis thaliana.** *Cell* 2016, **166:**481-491.

31. Sharbel TF, Haubold B, Mitchell-Olds T: **Genetic isolation by distance in Arabidopsis thaliana: biogeography and postglacial colonization of Europe.** *Mol Ecol* 2000, **9:**2109-2118.

32. Filiz E, Ozdemir BS, Budak F, Vogel JP, Tuna M, Budak H: **Molecular, morphological, and cytological analysis of diverse Brachypodium distachyon inbred lines.** *Genome* 2009, **52:**876-890.

33. Ng PC, Henikoff S: **SIFT: Predicting amino acid changes that affect protein function.** *Nucleic Acids Research* 2003, **31:**3812-3814.

34. Minadakis N, Williams H, Horvath R, Caković D, Stritt C, Thieme M, Bourgeois Y, Roulin AC: **The demographic history of the wild crop relative Brachypodium distachyon is shaped by distinct past and present ecological niches.** *Peer Community Journal* 2023, **3:**e84.

35. Stritt C, Gimmi EL, Wyler M, Bakali AH, Skalska A, Hasterok R, Mur LAJ, Pecchioni N, Roulin AC: **Migration without interbreeding: Evolutionary history of a highly selfing Mediterranean grass inferred from whole genomes.** *Mol Ecol* 2022, **31:**70-85.

36. Schmitz RJ, Schultz MD, Urich MA, Nery JR, Pelizzola M, Libiger O, Alix A, McCosh RB, Chen H, Schork NJ, Ecker JR: **Patterns of population epigenomic diversity.** *Nature* 2013, **495:**193-198.

37. Briffa A, Hollwey E, Shahzad Z, Moore JD, Lyons DB, Howard M, Zilberman D: **Millennia-long epigenetic fluctuations generate intragenic DNA methylation variance in Arabidopsis populations.** *Cell Syst* 2023, **14:**953-967 e917.

942 38. Taudt A, Roquis D, Vidalis A, Wardenaar R, Johannes F, Colome-Tatche M:
943 **METHimpute: imputation-guided construction of complete methylomes**
944 **from WGBS data.** *BMC Genomics* 2018, **19:**444.
945 39. Xia J, Han L, Zhao Z: **Investigating the relationship of DNA methylation with**
946 **mutation rate and allele frequency in the human genome.** *BMC Genomics*
947 2012, **13:**S7.
948 40. Mugal CF, Ellegren H: **Substitution rate variation at human CpG sites**
949 **correlates with non-CpG divergence, methylation level and GC content.**
950 *Genome Biol* 2011, **12:**R58.
951 41. Kusmartsev V, Drozdz M, Schuster-Bockler B, Warnecke T: **Cytosine Methylation**
952 **Affects the Mutability of Neighboring Nucleotides in Germline and Soma.**
953 *Genetics* 2020, **214:**809-823.
954 42. Stuart T, Eichten SR, Cahn J, Karpievitch YV, Borevitz JO, Lister R: **Population**
955 **scale mapping of transposable element diversity reveals links to gene**
956 **regulation and epigenomic variation.** *Elife* 2016, **5:**e20777.
957 43. Shen Y, Zhang J, Liu Y, Liu S, Liu Z, Duan Z, Wang Z, Zhu B, Guo YL, Tian Z: **DNA**
958 **methylation footprints during soybean domestication and improvement.**
959 *Genome Biol* 2018, **19:**128.
960 44. Eichten SR, Briskine R, Song J, Li Q, Swanson-Wagner R, Hermanson PJ, Waters
961 AJ, Starr E, West PT, Tiffin P, et al: **Epigenetic and genetic influences on DNA**
962 **methylation variation in maize populations.** *Plant Cell* 2013, **25:**2783-2797.
963 45. Zhao T, Guan X, Hu Y, Zhang Z, Yang H, Shi X, Han J, Mei H, Wang L, Shao L, et al:
964 **Population-wide DNA methylation polymorphisms at single-nucleotide**

965 **resolution in 207 cotton accessions reveal epigenomic contributions to**
966 **complex traits.** *Cell Res* 2024.
967 46. Avramidou EV, Korakaki E, Malliarou E, Boutsios S: **Studying the Genetic and**
968 **the Epigenetic Diversity of the Endangered Species Juniperus drupacea**
969 **Labill. towards Safeguarding Its Conservation in Greece.** *Forests* 2023,
970 **14:**1271.
971 47. Avramidou EV, Moysiadis T, Ganopoulos I, Michailidis M, Kissoudis C, Valasiadis
972 D, Kazantzis K, Tsaroucha E, Tsaftaris A, Molassiotis A, et al: **Phenotypic,**
973 **Genetic, and Epigenetic Variation among Diverse Sweet Cherry Gene Pools.**
974 *Agronomy* 2021, **11:**680.
975 48. Wang MZ, Li HL, Li JM, Yu FH: **Correlations between genetic, epigenetic and**
976 **phenotypic variation of an introduced clonal herb.** *Heredity (Edinb)* 2020,
977 **124:**146-155.
978 49. Langford N, Fargeot L, Blanchet S: **Spatial covariation between genetic and**
979 **epigenetic diversity in wild plant and animal populations: a meta-analysis.** *J*
980 *Exp Biol* 2024, **227**.
981 50. Medrano M, Alonso C, Bazaga P, Lopez E, Herrera CM: **Comparative genetic and**
982 **epigenetic diversity in pairs of sympatric, closely related plants with**
983 **contrasting distribution ranges in south-eastern Iberian mountains.** *AoB*
984 *Plants* 2020, **12:**plaa013.
985 51. Fargeot L, Loot G, Prunier JG, Rey O, Veyssiere C, Blanchet S: **Patterns of**
986 **Epigenetic Diversity in Two Sympatric Fish Species: Genetic vs.**
987 **Environmental Determinants.** *Genes (Basel)* 2021, **12:**107.

988 52. Lele L, Ning D, Cuiping P, Xiao G, Weihua G: **Genetic and epigenetic variations**
989 **associated with adaptation to heterogeneous habitat conditions in a**
990 **deciduous shrub.** *Ecol Evol* 2018, **8:**2594-2606.
991 53. Durvasula A, Fulgione A, Gutaker RM, Alacakaptan SI, Flood PJ, Neto C,
992 Tsuchimatsu T, Burbano HA, Pico FX, Alonso-Blanco C, Hancock AM: **African**
993 **genomes illuminate the early history and transition to selfing in Arabidopsis**
994 **thaliana.** *Proc Natl Acad Sci U S A* 2017, **114:**5213-5218.
995 54. Lamesch P, Berardini TZ, Li D, Swarbreck D, Wilks C, Sasidharan R, Muller R,
996 Dreher K, Alexander DL, Garcia-Hernandez M, et al: **The Arabidopsis**
997 **Information Resource (TAIR): improved gene annotation and new tools.**
998 *Nucleic Acids Res* 2012, **40:**D1202-1210.
999 55. Danecek P, Bonfield JK, Liddle J, Marshall J, Ohan V, Pollard MO, Whitwham A,
1000 Keane T, McCarthy SA, Davies RM, Li H: **Twelve years of SAMtools and**
1001 **BCFtools.** *Gigascience* 2021, **10:**giab008.
1002 56. Nassar LR, Barber GP, Benet-Pages A, Casper J, Clawson H, Diekhans M, Fischer
1003 C, Gonzalez JN, Hinrichs AS, Lee BT, et al: **The UCSC Genome Browser**
1004 **database: 2023 update.** *Nucleic Acids Res* 2023, **51:**D1188-D1195.
1005 57. Bolger AM, Lohse M, Usadel B: **Trimmomatic: a flexible trimmer for Illumina**
1006 **sequence data.** *Bioinformatics* 2014, **30:**2114–2120.
1007 58. Krueger F, Andrews SR: **Bismark: a flexible aligner and methylation caller for**
1008 **Bisulfite-Seq applications.** *Bioinformatics* 2011, **27:**1571-1572.
1009 59. Lister R, O'Malley RC, Tonti-Filippini J, Gregory BD, Berry CC, Millar AH, Ecker JR:
1010 **Highly integrated single-base resolution maps of the epigenome in**
1011 **Arabidopsis.** *Cell* 2008, **133:**523-536.

1012 60. Hazarika RR, Serra M, Zhang Z, Zhang Y, Schmitz RJ, Johannes F: **Molecular**
1013 **properties of epimutation hotspots.** *Nat Plants* 2022, **8:**146-156.
1014 61. Williams CJ, Dai D, Tran KA, Monroe JG, Williams BP: **Dynamic DNA methylation**
1015 **turnover in gene bodies is associated with enhanced gene expression**
1016 **plasticity in plants.** *Genome Biol* 2023, **24:**227.
1017 62. Hamala T, Tiffin P: **Biased Gene Conversion Constrains Adaptation in**
1018 **Arabidopsis thaliana.** *Genetics* 2020, **215:**831-846.
1019 63. Paradis E: **pegas: an R package for population genetics with an integrated-**
1020 **modular approach.** *Bioinformatics* 2010, **26:**419-420.
1021 64. Danecek P, Auton A, Abecasis G, Albers CA, Banks E, DePristo MA, Handsaker
1022 RE, Lunter G, Marth GT, Sherry ST, et al: **The variant call format and VCFtools.**
1023 *Bioinformatics* 2011, **27**.
1024 65. Zhang C, Dong SS, Xu JY, He WM, Yang TL: **PopLDdecay: a fast and effective**
1025 **tool for linkage disequilibrium decay analysis based on variant call format**
1026 **files.** *Bioinformatics* 2019, **35:**1786-1788.
1027 66. Lefort V, Desper R, Gascuel O: **FastME 2.0: A Comprehensive, Accurate, and**
1028 **Fast Distance-Based Phylogeny Inference Program.** *Mol Biol Evol* 2015,
1029 **32:**2798-2800.
1030 67. Yu G, Smith DK, Zhu H, Guan Y, Lam TTY: **ggtree: an r package for visualization**
1031 **and annotation of phylogenetic trees with their covariates and other**
1032 **associated data.** *Methods in Ecology and Evolution* 2017, **8:**28-36.
1033 68. Jombart T: **adegenet: a R package for the multivariate analysis of genetic**
1034 **markers.** *Bioinformatics* 2008, **24:**1403–1405.

1035 69. Li H: **Aligning sequence reads , clone sequences and assembly contigs with**
1036 **BWA-MEM.** 2013, **00:**1-3.
1037 70. McKenna A, Hanna M, Banks E, Sivachenko A, Cibulskis K, Kernytsky A,
1038 Garimella K, Altshuler D, Gabriel S, Daly M, DePristo MA: **The Genome Analysis**
1039 **Toolkit: A MapReduce framework for analyzing next-generation DNA**
1040 **sequencing data.** *Genome Research* 2010, **20:**1297–1303.
1041 71. Niederhuth CE, Bewick AJ, Ji L, Alabady MS, Kim KD, Li Q, Rohr NA, Rambani A,
1042 Burke JM, Udall JA, et al: **Widespread natural variation of DNA methylation**
1043 **within angiosperms.** *Genome Biol* 2016, **17:**194.
1044 72. Sanchez T, Cury J, Charpiat G, Jay F: **Deep learning for population size history**
1045 **inference: Design, comparison and combination with approximate Bayesian**
1046 **computation.** *Mol Ecol Resour* 2021, **21:**2645-2660.
1047 73. Baumdicker F, Bisschop G, Goldstein D, Gower G, Ragsdale AP, Tsambos G, Zhu
1048 S, Eldon B, Ellerman EC, Galloway JG, et al: **Efficient ancestry and mutation**
1049 **simulation with msprime 1.0.** *Genetics* 2022, **220**.
1050 74. Paszke A, Gross S, Massa F, Lerer A, Bradbury J, Chanan G, Killeen T, Lin Z,
1051 Gimelshein N, Antiga L, et al: *pyTorch: An Imperative Style, High-Performance*
1052 *Deep Learning Library.* Curran Associates, Inc.; 2019.
1053 75. Shazeer N: **GLU Variants Improve Transformer.** *arXiv* 2020**:**2002.05202.
1054 76. He R, Ravula A, Kanagal B, Ainslie J: **RealFormer: Transformer Likes Residual**
1055 **Attention.** *arXiv* 2021**:**2012.11747.
1056 77. Su J, Ahmed M, Lu Y, Pan S, Bo W, Liu Y: **RoFormer: Enhanced transformer with**
1057 **Rotary Position Embedding.** *Neurocomputing* 2024, **568:**127063.

78. Gugger S, Debut L, Wolf T, Schmid P, Mueller Z, Mangrulkar S, Sun M, Bossan B: **Accelerate: Training and inference at scale made simple, efficient and adaptable.** *https://githubcom/huggingface/accelerate* 2022.